Coversheet

Title

An integrated approach for characterizing and selecting climate change scenarios: Focusing on variability and extremeness

Authors

- Jaeyoung Kim (Korea Environment Institute, jykim@kei.re.kr)
- Moon-Hwan Lee (Korea Environment Institute, mhlee@kei.re.kr)
- Jong-Ho Ahn (Korea Environment Institute, ahnjh@kei.re.kr)
- Seung-Beom Seo (University of Seoul, sbseo7@uos.ac.kr)

Preprint Statement

This manuscript is a non-peer reviewed preprint submitted to EarthArXiv. The manuscript is also currently under review at the journal *Climate Dynamics*. Please note that, despite being under peer review, the manuscript has not yet been formally accepted for publication. Subsequent versions of this manuscript may differ slightly from this version. If accepted, the final version will be available via the DOI of the journal publication. Please feel free to contact any of the authors; we welcome feedback.

An integrated approach for characterizing and selecting climate change scenarios: Focusing on variability and extremeness

Jaeyoung Kim[1], Moon-Hwan Lee[1], Jong-Ho Ahn[1], Seung-Beom Seo[2]*

[1]Division for Integrated Water Management, Water and Land Research Group, Korea Environment Institute, Republic of Korea

[2]International School of Urban Sciences, University of Seoul, Seoul, Republic of Korea

*Corresponding author: Seung-Beom Seo (sbseo7@uos.ac.kr)

Abstract

This study presents a novel integrated approach for selecting optimal combinations of global climate models (GCMs) and shared socioeconomic pathways (SSPs) to assess the impact of climate change on the aquatic environment. The method proposed in this study considers the comprehensive spatial and temporal ranges of climate projections, specifically focusing on the variability and extremeness of climate change across all accessible regions and timescales. This approach uses entropy and frequency analyses to integrate multiple climate indices related to precipitation and air temperature into a single metric representing the unique variability and extreme characteristics of each scenario. In this study, 35 GCM-SSP combinations were analyzed, yielding the following major findings. While variability and extremeness in climate scenarios tended to increase under severe global warming scenarios, this trend was not always consistent. These findings suggest that the general insights into GCMs and SSPs should be broadened. Suitable GCM-SSP combinations were selected by ranking unique characteristics using the Katsavounidis-Kuo-Zhang algorithm, enabling the capture of the full range of GCM-SSP combinations with a minimal number of combinations. Although precipitation and air temperature were the primary focus, the method can be expanded to include other weather variables, such as wind speed and solar radiation. The results demonstrate that this integrated approach effectively represents a wide range of climate scenarios, providing a comprehensive understanding of the projected climates across different regions and timescales. By transforming high-dimensional data into a single dimension, this approach simplifies interpretation, supporting a more effective identification of GCM-SSP combinations suitable for diverse climate adaptation strategies.

Keywords: Climate Change, Entropy, Variability, Extremeness, Dimensionality Reduction

1. Introduction

The development of climate change adaptation strategies for various sectors must be grounded in the projected future conditions. However, achieving a uniform projection of the future climate is inherently challenging owing to the randomness and uncertainty of real-world conditions. In climate change assessment research, it is a common practice to employ various global climate models (GCMs) to capture the full range of possible scenarios (Lutz et al., 2016; Najafi and Moradkhani, 2015; Seo et al., 2019). However, this approach incurs high computational and temporal costs. The Coupled Model Intercomparison Project Phase 6 (CMIP6) provides access to more than 120 published GCMs (wcrp-cmip.org). Combined with the four representative shared socioeconomic pathway (SSP)–representative concentration pathway (RCP) scenarios—SSP126, SSP245, SSP370, and SSP585—this resulted in a wide range of SSP-RCP combinations across multiple GCMs. Therefore, selecting the optimal GCM-SSP combination is essential to balance a comprehensive analysis with computational efficiency.

The direction of GCM and SSP selections can be divided into two categories: (1) models that accurately reproduce historical climate patterns and (2) models that project plausible future climate patterns (Vano et al., 2015). The former can be evaluated based on the accuracy of reproducing daily, seasonal, and annual cycle patterns compared with observations (e. g., Biemans et al., 2013; Lutz et al., 2016; Samadi et al., 2010). Although this is an important procedure, it does not guarantee that a model with high historical accuracy will provide plausible climate projections or capture the full range of potential future events (McSweeney et al., 2015; Mendlik and Gobiet, 2016). Furthermore, although officially certified and published by CMIP6 ensures a certain level of reliability in reproducing past climate patterns (Stocker et al., 2013), the accuracy of GCMs varies across regions. Under these conditions, the selection of GCMs and SSPs is based on the evaluation of projected climate characteristics such as changes, variability, and extremeness.

A simple method for selecting climate change scenarios involves using specific combinations of GCMs and SSPs. Although this approach has the lowest cost, it may lead to biased or nonuniform distributions in the projected results. The change rate can be used as a single value comparing future data to historical data; however, it has limitations in reflecting specific climate characteristics, such as variability, extremeness, and frequency. The clustering approach has been applied to reduce the number of GCMs or SSPs by grouping similar subclusters of future projections (Carvalho et al., 2016;

Lee and Kim, 2012; Mahlstein and Knutti, 2010). However, the clustering approach primarily identifies GCM scenarios that represent the central tendency of each sub-cluster rather than capturing the full range of variability within the ensemble (Cannon, 2015). To capture the range of projected climate extremeness, many researchers have applied extreme climate indices (ECIs; Cannon, 2015; Farjad et al., 2019; Hong and Ying, 2018; Lutz et al., 2016; Seo et al., 2019), which represent the 27 indicators proposed by the World Meteorological Organization's Expert Team on Climate Change Detection and Indices (ETCCDI; Zhang et al., 2011). However, ECI results in high-dimensional combinations, leading to complexity. Additionally, cross-correlation between ECIs can cause redundancy, which is expressed as multicollinearity (Farjad et al., 2019; Seo et al., 2019). The Katsavounidis (KKZ) Zhang algorithm (Katsavounidis et al., 1994) has been widely applied (Cannon, 2015; Farjad et al., 2019; Qian et al., 2021; Ross and Najjar, 2019; Seo et al., 2019). Unlike k-means clustering, the KKZ algorithm recursively selects models that best cover the range of an ensemble, effectively representing high-density regions within multivariate space (Katsavounidis et al., 1994). Model selection is based on the model furthest from the previously selected one; therefore, there is no guarantee that the most extreme scenario will be chosen during this process (Farjad et al., 2019). For suitable scenario selection, the datasets for the KKZ algorithm should be prepared in the analysis direction.

Many studies using established methodologies for scenario selection have focused on either a single or integrated site based on averages and specific future periods. Because this approach emphasizes a particular region or period of interest, the method of integrating a region or time can vary significantly across studies. In response to these variations, this study proposes a novel integrated approach for selecting plausible climate change scenarios. This approach focused on the variability and extremeness of climate change across all accessible regions and over the entire period. Specifically, the inclusion of accessible GCMs, SSPs, regions, time periods, and indices results in a high-dimensional dataset, increasing the complexity and making interpretation more challenging. The method proposed in this study integrates these high dimensions into a single dimension, creating integrated values that uniquely represent the variability in diverse weather information and the extremeness of weather conditions for each climate change scenario. This process simplifies the understanding of the characteristics of each scenario. Additionally, analyzing the distribution range of these quantified characteristic values provides valuable insights into the expected future climate impacts, aiding the development of climate change adaptation strategies.

2. Material and methods

2.1. Frameworks

This research was conducted to identify suitable GCM-SSP combinations for climate change assessment in aquatic environments. The determination procedure consisted of five steps, as shown in Figure 1. The first step involved identifying a representative site for determining ECIs. This was accomplished by selecting a site with minimal fluctuations in historical climate data and using Entropy Analysis to ensure stable historical conditions. This site provides a robust basis for correlation analyses between the identified ECIs derived from historical data. Second, the number of ECIs at the identified site was optimized. In this step, specific ECIs that exhibited a high correlation and multicollinearity with other ECIs were excluded. The third step quantifies the future variability of the spatiotemporal ECIs for each GCM-SSP combination. The high-dimensional state arising from the ECI type, time, and location was reduced to a single value using two approaches: (1) the Entropy Weight method and (2) the Multivariate Entropy method. The fourth step quantifies the future extremeness of the spatiotemporal ECIs for each GCM-SSP combination. Similar to the third step, the high-dimensional state was reduced to a single value using a frequency analysis, which quantified the occurrence of extreme events across multiple regions and over extended periods. The fifth step determines suitable GCM-SSP combinations using the KKZ algorithm, incorporating the results of the third and fourth steps. These procedures integrate uncertainty and extremeness across time and space within a large climate-data environment. Determining the optimal GCM-SSP combinations reduces the need to analyze numerous scenario combinations.

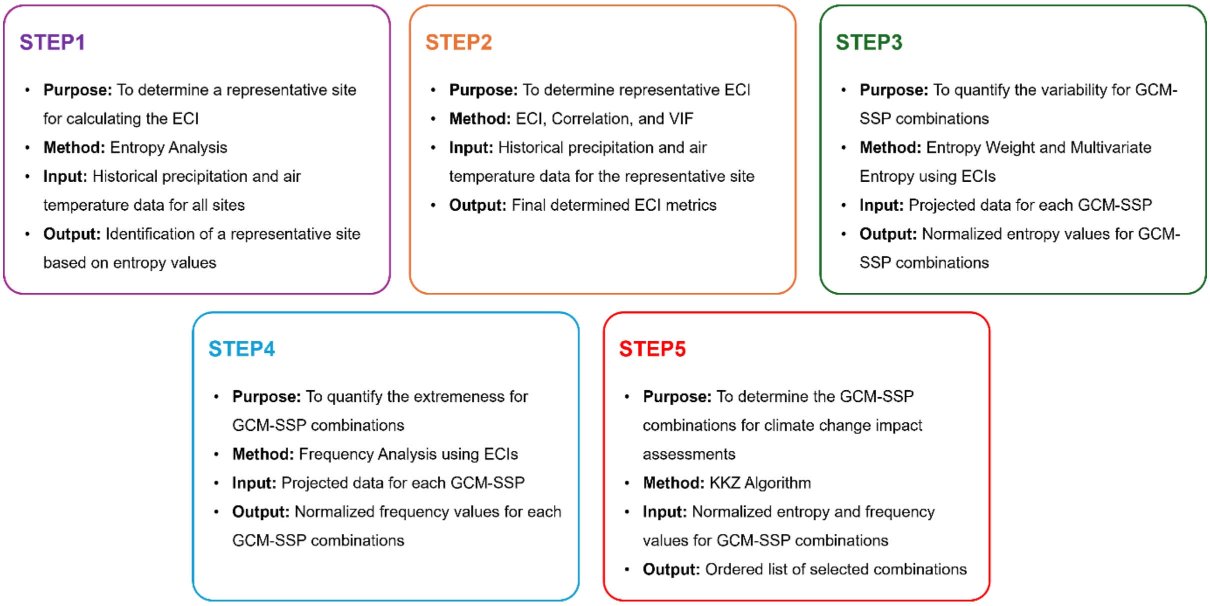

Figure 1. Frameworks for characterizing and selecting GCM-SSP combinations.

2.2. Study area: Republic of Korea

The spatial range for the proposed approach to determine the GCM-SSP combinations was the Republic of Korea (hereafter, South Korea). South Korea covers an area of approximately 100,000 km^2 and includes five main river basins, as shown in Figure 2(A). The country is primarily influenced by the climatic conditions of the Asian monsoon, with approximately two-thirds of the annual precipitation occurring during the flood season, which spans from July to September. In contrast, severe dry periods occurred during the drought season from October to June. Figure 2-(B) shows the Thiessen polygons for the precipitation gauges (Thiessen, 1911). In this study, the projected data were extracted from the center of each polygon, totaling 601 sites collectively covering South Korea.

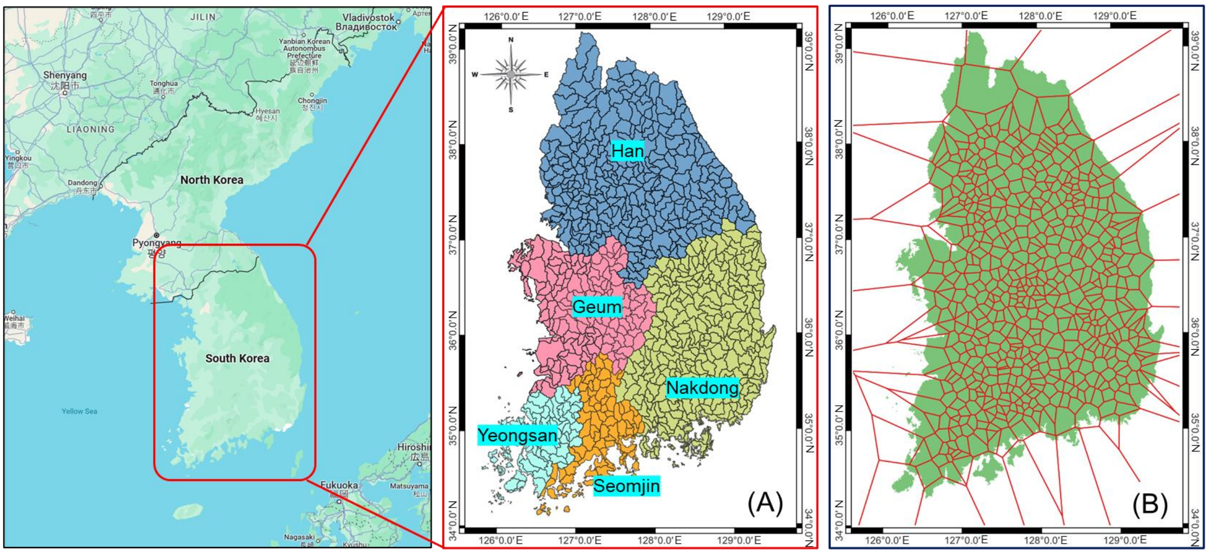

Figure 2. Study area: South Korea. (A) 5 river basins and subbasins, and (B) Thiessen polygons for rain gauges.

2.3. GCM data sets

In this study, seven GCMs and five SSP scenarios were used, including SSP119. The selected GCMs are CanESM5 (Can), EC-Earth3 (EC), GFDL-ESM4 (GFDL), IPSL-CM6A-LR (IPSL), MIROC6 (MIR), MPI-ESM1-2-LR (MPI), and MRI-ESM2-0 (MRI), while the SSP scenarios include SSP119, SSP126, SSP245, SSP370, and SSP585. Under these conditions, 35 GCM-SSP combinations were created. Table 1 presents detailed information on the GCMs and SSP scenarios. Large-scale data from each GCM were downscaled to a regional scale of 1 km × 1 km using the method developed by Eum et al. (2018). This method incorporates an adaptive radius of influence that is adjusted based on the density of available climate stations, enabling high-resolution interpolation that accounts for local physiographic factors, such as elevation and proximity to coastlines. By employing this approach, downscaling achieved a 1 × 1 km resolution, effectively capturing regional climate variability and improving accuracy in areas with complex topography, as demonstrated by Eum et al. (2018). The downscaled projected data of the GCM-SSP combinations included historical simulations for 1981–2010 and future projections for 2011–2100. These combinations included daily datasets of (1) precipitation, (2) maximum temperature, (3) minimum temperature, (4) relative humidity, (5) solar radiation, and (6) wind speed. In this study, precipitation and air temperature data extracted from 601 sites within the Thiessen polygon were used to determine GCM-SSP combinations, considering that precipitation and air temperature are the dominant factors affecting water resource management.

Table 1. Detailed information of GCMs and SSPs used in this study.

No.	GCM model	SSP Scenario	Original resolution (Number of grids)	Downscaled resolution	Reference
1	CanESM5 (Can5)	SSP119 SSP126 SSP245 SSP370 SSP585	128 x 64	1 km x 1 km	Swart et al., 2019
2	EC-Earth3 (EC3)		512 x 256		Döscher et al., 2021
3	GFDL-ESM4 (GFDL)		360 x 180		Dunne et al., 2020
4	IPSL-CM6A-LR (IPSL)		144 x 143		Boucher et al., 2020
5	MIROC6 (MIR6)		256 x 128		Tatebe et al., 2019
6	MPI-ESM1-2-LR (MPI)		192 x 96		Mauritsen et al., 2019
7	MRI-ESM2-0 (MRI)		320 x 160		Yukimoto et al., 2019

2.4. Extreme Climate Index

The ECIs of the ETCCDI for precipitation and air temperature are useful for analyzing climate extremes. They provide a comprehensive understanding of climatic conditions by focusing on the extreme aspects (Zhang et al., 2011). Therefore, ECIs have been applied in various studies on climatic conditions, including climate change research (Cooley and Chang, 2021; Hong and Ying, 2018; Seo and Kim, 2018; Seo et al., 2019). This study used ECIs, which include 26 indices for extreme aspects of precipitation and air temperature, as shown in Table 2.

Each ECI can explain extreme climatic conditions; however, their explanations can be redundant if a strong correlation exists between them. Therefore, it is not necessary to consider every ECI unless all ECIs are independent (Seo et al., 2019). In this study, correlation analysis and the variance inflation factor (VIF) were used to determine suitable ECIs. If the Pearson correlation between two ECIs was greater than 0.7 or less than -0.7, the ECI with the least correlation with the other ECIs was selected (i.e., the most independent ECI). Subsequently, to prevent multicollinearity among ECIs, a final ECI combination with a VIF of < 5 was determined. Through this procedure, representative ECIs were identified, and the ECI values of the ECIs are calculated annually from 2021 to 2100, spanning 80 years.

Table 2. Definitions of the 26 ECIs for precipitation and air temperature.

Variable	Index	Definition
Precipitation	Rx1day	Annual maximum 1-day precipitation
	Rx5day	Annual Maximum consecutive 5-day precipitation
	SDII	Simple precipitation intensity index: mean precipitation amounts on wet days (≥ 1 mm)
	R10mm	Annual count of days with precipitation ≥ 10 mm
	R20mm	Annual count of days with precipitation ≥ 20 mm
	R50mm	Annual count of days with precipitation ≥ 50 mm
	CDD	Maximum length of dry spell: maximum number of consecutive days with < 1 mm precipitation
	CWD	Maximum length of wet spell: maximum number of consecutive days with ≥ 1 mm precipitation
	R95ptot	Annual total precipitation when daily wet day amount > 95th percentile
	R99ptot	Annual total precipitation when daily wet day amount > 99th percentile
	PRCPTOT	Annual total precipitation in wet days
Air temperature	SU	Annual count of days when maximum temperature > 25°C
	ID	Annual count of days when maximum temperature < 0°C
	TXn	Annual minimum value of maximum temperature
	TXx	Annual maximum value of maximum temperature
	TX10p	Percentage of days when maximum temperature < 10^{th} percentile
	TX90p	Percentage of days when maximum temperature > 90^{th} percentile
	WSDI	Annual count of days with at least 6 consecutive days when maximum temperature > 90^{th} percentile
	FD	Annual count of days when minimum temperature < 0°C
	TR	Annual count of days when minimum temperature > 20°C
	TNn	Annual minimum value of minimum temperature
	TNx	Annual maximum value of minimum temperature
	TN10p	Percentage of days when minimum temperature < 10^{th} percentile
	TN90p	Percentage of days when minimum temperature > 90^{th} percentile
	CSDI	Annual count of days with at least 6 consecutive days when minimum temperature < 10^{th} percentile
	DTR	Daily temperature range: mean difference between maximum and minimum temperature

2.5. Information entropy for quantifying variability

Shannon (1948) introduces the concept of information entropy for information diversity and uncertainty. In this theory, data disorder provides a large amount of information that can be expressed as high entropy. In other words, inconsistent events provide a wide range of experiences and information. The Shannon entropy is defined as follows:

$$H(X) = -\sum_{i=1}^{n} p(x_i) \log_2 p(x_i) \qquad \text{Equation 1}$$

Where H is Shannon entropy, X is a variable, p is the probability of the i^{th} event, and x_i is the i^{th} value of the variable. The diversity or uncertainty of data can be quantified as a single value using the entropy method. Furthermore, it can reduce the dimensionality of the datasets. In this study, two methods were used for dimensionality reduction: (1) the entropy weight method and (2) the multivariate entropy methods.

The entropy weight method integrates datasets for multiple variables into one integrated variable by using the entropy weight value for each variable. The calculation procedure for the entropy weight method consists of four steps.

① Data normalization

The dataset for each variable was normalized to a range of 0 to 1, ensuring uniform dimensions among the variables. This procedure was conducted using min–max normalization.

② Calculation of Information entropy for each variable

$$H_j = -\frac{1}{\ln m} \sum_{i=1}^{m} v_{ij} \ln v_{ij} \qquad \text{Equation 2}$$

Where H_j is the entropy value of j^{th} variable, m the number of data points, and v_{ij} the probability of j^{th} variable for i^{th} event.

③ Entropy weight calculations

$$W_j = \frac{H_j}{\sum_{j=1}^{m} H_j} \qquad \text{Equation 3}$$

Where W_j denotes the entropy weight of j^{th} variable. In general, entropy weight is calculated using $1 - H_j$ instead of H_j. This implies that data with low uncertainty have a high weight. However, in this study, it was assumed that the data with high uncertainty had a high weight. This approach is intended to include as much information as possible regarding climate change scenarios.

④ Variable integration

In this step, the normalized data were multiplied by the entropy weight of each variable. Subsequently, all multiplied-normalized data were added. This procedure results in an integrated dataset that accounts for all the variables and their respective weights.

For instance, the multivariate entropy for three variables is defined as follows:

$$H(X,Y,Z) = -\sum_{i=1}^{n} p(x_i, y_i, z_i) \log_2 p(x_i, y_i, z_i) \qquad \text{Equation 4}$$

Equation 4 calculates the integrated entropy for variables X, Y, and Z. The multivariate entropy was calculated based on the joint probability distribution, reflecting the correlations and interactions among multiple variables. In this procedure, the datasets for the three variables are reduced to a single value, thereby achieving dimensionality reduction.

In this study, the entropy weight method was used to integrate representative ECIs into a single integrated ECI (i.e., a single index) to reduce the dimensionality of the representative ECIs. In this step, each GCM-SSP combination had datasets for the integrated ECI spanning 80 years and covering 601 locations. Subsequently, the multivariate entropy method integrated the time and location data for the integrated datasets of each GCM-SSP combination and calculated the final entropy value representing each GCM-SSP combination.

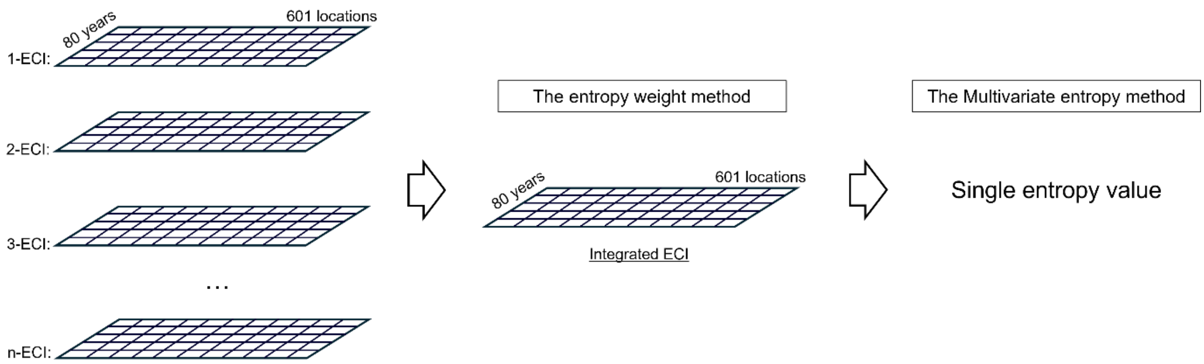

Figure 3. Procedures for quantifying the variability of each GCM-SSP combination using the entropy weight and multivariate entropy methods.

2.6. Katsavounidis-Kuo-Zhang (KKZ) algorithm for scenario selection

The KKZ algorithm (Katsavounidis et al., 1994) was used to select the GCM-SSP combination based on its entropy value. Unlike k-means clustering, the KKZ algorithm recursively selects models that best span the spread of an ensemble, effectively characterizing high-density regions in a multivariate space (Katsavounidis et al., 1994; Seo et al., 2019). Scenario selection using the KKZ algorithm consisted of four steps.

① The first scenario is the closest to the ensemble centroid. The location was calculated using the sum of the squared errors, as shown in Equation 5:

$$SSE = \sum_{p=1}^{P} \sum_{i=1}^{N} \left(y_{ip} - y_p\right)^2 \quad \text{Equation 5}$$

where y_{ip} is the value of the pth variable for the ith scenario and y_p is the centroid value of the pth

variable across all scenarios.

② The second scenario is the one that is located furthest from the first scenario. The location was calculated using the Euclidean distance.

③ The distances between the remaining scenarios and the previously selected models were calculated. For each remaining scenario, only the shortest distance from any previously selected model was retained. The scenario with the longest retention distance was determined as the next scenario. This procedure was repeated until the final scenario was obtained.

The KKZ algorithm selects suitable GCM-SSP combinations, enabling the capture of the full range of GCM-SSP combinations with a minimal number of combinations.

3. Results and Discussion

3.1. Determination of representative site and ECIs

3.1.1. Representative site

This section focuses on determining the representative sites for the selection of representative ECIs. To calculate the information entropy for precipitation and air temperature, past daily data from 601 sites covering 2000 to 2019 were used. Figure 4 shows the calculated multivariate entropy for the variability of past precipitation and mean air temperature, with values ranging from 6.71 to 7.44 and an average of 7.08. The representative ECI site was identified as the site with the lowest entropy value. A low entropy indicates low variability and uncertainty, signifying stable data conditions. These stable conditions facilitate statistical significance due to low variance, resulting in narrower confidence intervals (Greenland et al., 2016; Poole, 2001). Therefore, the procedures for determining ECIs at a representative site can be considered reliable owing to the robustness of past data.

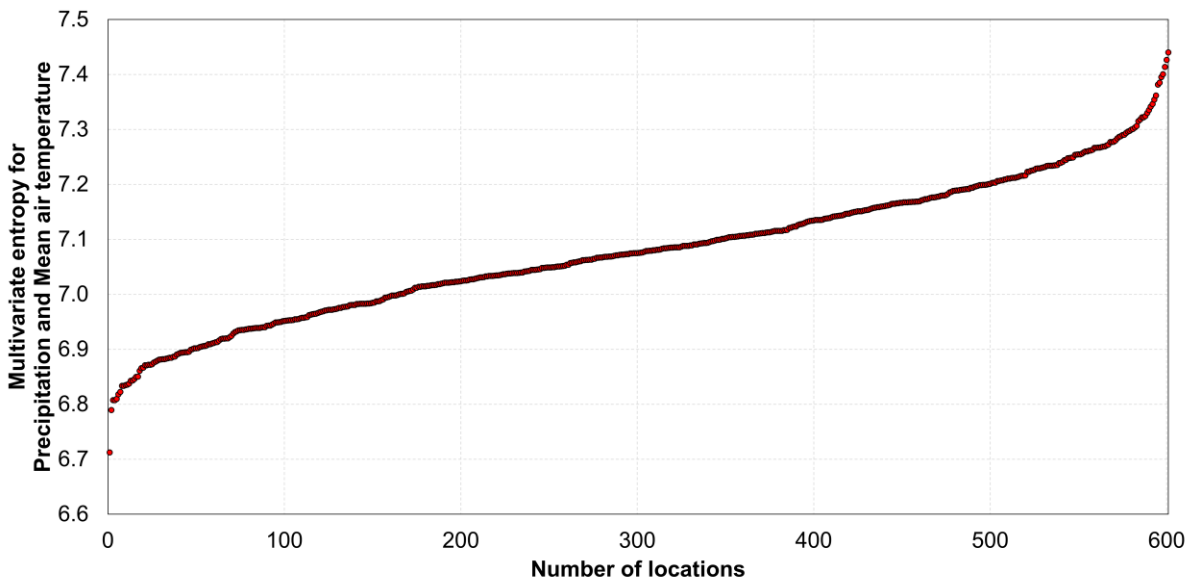

Figure 4. Information entropy for past precipitation from 2000 to 2019.

3.1.2. Representative ECIs

The 26 ECIs related to precipitation and air temperature were calculated from past data of a representative site. Figure 5 shows the results of the correlation analysis among these ECIs, revealing that most ECIs exhibited strong correlations with one another. In particular, the PRCPTOT and SDII were strongly correlated with the other ECIs.

Based on these results, multi-collinearity among these ECIs could diminish the explanatory power of the representativeness of the GCM-SSP combinations. To address this issue, ECIs with correlation values greater than 0.7 or less than -0.7 with other ECIs were identified and sorted. Among these, the ECI with the most connections to other ECIs were excluded. The excluded ECIs related to precipitation were Rx1day, SDII, R20 mm, R50 mm, R95ptot, R99ptot, and PRCPTOT. The excluded ECIs related to air temperature were SU, ID, TXn, TX10p, TX90p, FD, TR, TNx, TN10p, TN90p, and CSDI. multi-collinearity among the selected ECIs was then checked using the VIF method, yielding the following values: (1) precipitation-related ECIs: Rx5day 1.88, R10mm 1.64, CDD 1.48, and CWD 1.72, and (2) four air-temperature-related ECIs: TXx 1.36, TNn 1.16, WSDI 1.34, and DTR 1.20. Therefore, the representativeness of each GCM-SSP combination was evaluated based on the eight ECIs that satisfied statistical significance.

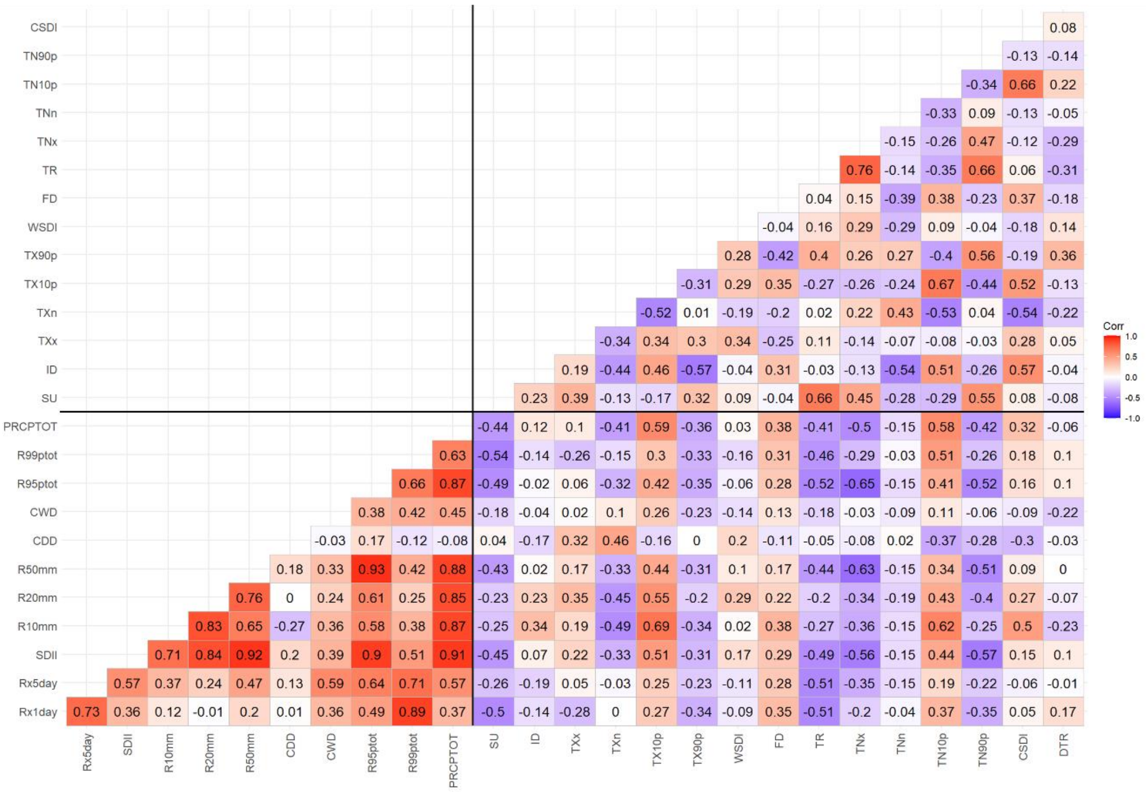

Figure 5. Correlation coefficient table across 26 ECIs for precipitation and air temperature.

3.2. Characteristic quantification for GCM-SSP combinations

3.2.1. Variability quantification

In the concept of information entropy, data variability refers to the extent to which information related to the projected precipitation and air temperature is diverse. Projected data with high entropy values can provide a substantial range of information regarding future weather conditions. In this study, entropy calculations for the data variability of each GCM-SSP combination consisted of three steps. In the first step, the eight selected ECIs were calculated for 80 years and 601 sites within each GCM-SSP combination. In this step, each combination resulted in a total of 8 x 80 x 601 data points.

Second, the eight ECIs were integrated into a single index using the entropy weight method. In this step, each combination yields 80 × 601 data points. To integrate a single index, the entropy weight for each ECI was calculated based on individual entropy values. An ECI with a high entropy value corresponded to a high-entropy weight. Table 3 presents comprehensive information regarding the entropy weights of the eight ECIs. The ranks in Table 3 indicate the order of the highest weights, while the number corresponding to each rank represents the count of values where the weight of each ECI for each GCM-SSP combination falls. Individual ranking was assigned to the maximum number of combinations, which was 35. Among the eight ECIs, DTR was mostly ranked 1st, with an average weight of 0.146, indicating that DTR provides the most information on climate change scenarios. Rx5day was mostly ranked 2nd, also with an average weight of 0.146, although its value was slightly different from the DTR when considering the decimal points. This similarity suggests that the explanatory powers of the two ECIs were comparable. TNn and TXx ranked 3rd and 4th, respectively, with average weights of 0.145. This result was comparable to the similarity observed between DTR and Rx5day. The next-ranked ECIs were WSDI, CDD, R10mm, and CWD. Notably, the WSDI had the highest distribution range of 0.055 between its maximum and minimum values, although its weight was not the highest. This suggests that the WSDI can still be considered a key index for characterizing each GCM-SSP combination, while its distribution stands out in contrast to the relatively stable differences observed in the other ECIs.

Table 3. The number of rank and statistical values for entropy weights of 35 GCM-SSP combinations.

Rank	Precipitation				Air temperature			
	Rx5day	R10mm	CDD	CWD	TXx	TNn	WSDI	DTR
1	14	0	0	0	0	0	0	21
2	21	0	0	0	0	0	0	14
3	0	0	0	0	6	29	0	0
4	0	0	0	0	29	6	0	0
5	0	1	5	0	0	0	29	0
6	0	12	21	0	0	0	2	0
7	0	22	9	1	0	0	3	0
8	0	0	0	34	0	0	1	0
Mean	0.146	0.106	0.108	0.082	0.145	0.145	0.121	0.146
Diff.*	0.012	0.008	0.014	0.018	0.011	0.011	0.055	0.012

Diff.: Difference (Maximum – Minimum)

In the final step, a single entropy value for the integrated index encompassing all time periods and sites within each GCM-SSP combination was calculated using the multivariate entropy method. In this step, the spatiotemporal data variability was consolidated into a representative value. Figure 6 shows the entropy values for the variability of the integrated ECI for each GCM-SSP combination. As shown in Figure 6(A), the mean entropy for MPI was the highest at 2.16, compared to the other GCMs. Simultaneously, the minimum entropy was observed for MPI-SSP119, whereas the maximum entropy was recorded for IPSL-SSP370. This indicates that the model provides the most information in terms of data variability. The entropy values for IPSL were widely and evenly distributed with a maximum entropy value. This suggests that IPSL combinations provide information on a diverse range of events as well as on the recurrence of similar or identical events.

The entropy values for the integrated ECI of each GCM-SSP combination were normalized to the range of one–two, as shown in Figure 6(B). The values steadily decreased from IPSL-SSP370 to MIR6-SSP245, followed by a significant decline. The highest value was observed for IPSL-SSP370, while the lowest was observed for MRI-SSP119, suggesting that MRI-SSP119 can project stable climatic conditions. Most entropy values for the same GCM increased as the scenario progressed from SSP119 to SSP585. However, these trends were not consistent across all the GCMs. The maximum entropy was observed for IPSL-SSP370, and for MRI, the highest entropy was observed for SSP370. The EC3 value for SSP119 was higher than that for SSP126. Additionally, the entropy values for MIR6 did not follow a consistent trend across SSP scenarios. This suggests that the SSP585 scenario, which is associated with severe global warming, does not always result in the greatest variability in extreme precipitation and air temperature for all the GCMs. Similarly, the SSP119 scenario, which emphasizes the mitigation of global warming, does not always lead to low variability. Previous studies on the variability of projected climate conditions have shown that (1) variability increases significantly in the SSP585 scenario (Almazroui et al., 2021; de Vries et al., 2024; Zarrin and Dadashi-Roudbari, 2021; Zhu et al., 2021), and (2) variability does not always increase under the SSP585 scenario and is region-dependent (Chen and Sun, 2021; Ghazi and Jeihouni, 2022; Wei et al., 2023; Zou and Zhou, 2022). Therefore, relying solely on the most severe level of global warming (e.g., SSP585) is not always suitable for providing a complete picture of potential changes in precipitation and air temperature.

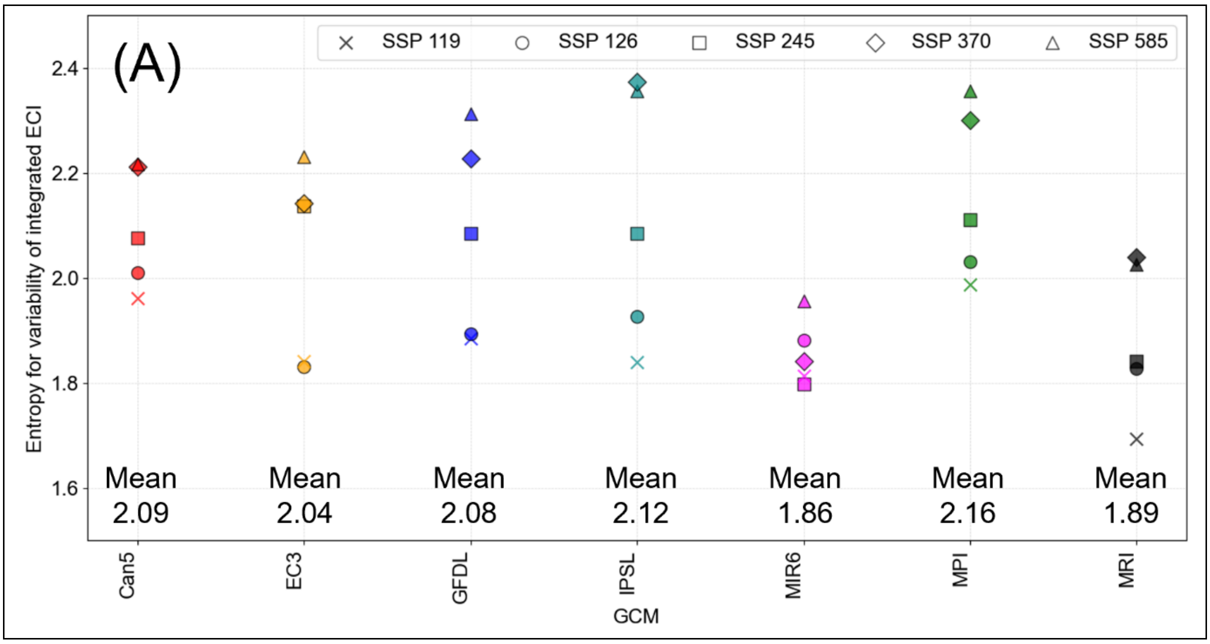

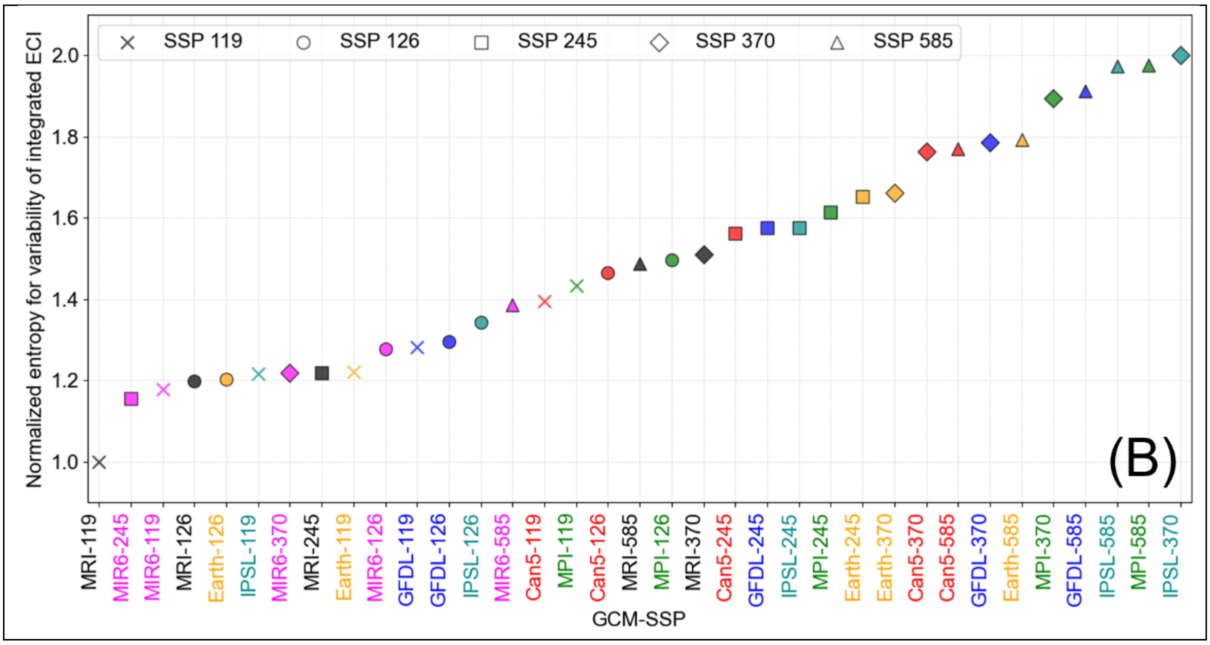

Figure 6. Entropy analysis results for variability of integrated ECI. (A) Entropy values and (B) Normalized entropy values.

3.2.2. Extremeness quantification

To quantify the extremeness of each GCM-SSP combination, a frequency analysis method using eight ECIs was applied. In Section 3.2.1, eight ECIs were calculated for 80 years and 601 sites within each GCM-SSP combination. The average of each ECI across 601 sites was obtained, resulting in 8 × 80 data points for each GCM-SSP combination. The dataset was then divided into 10 groups, with the "1st" group representing the lowest extremeness and the "10th" group representing the highest extremeness. Table 4 shows the decile distribution for the eight ECIs of all GCM-SSP combinations (80 × 35 data points for each ECI). The ECIs related to precipitation were primarily distributed within the 1st to 5th deciles, with a significant decrease observed as the values approached the highest extreme levels, as represented by the 10th decile. For the ECIs related to air temperature, TXx and DTR were primarily distributed in the 3rd to 5th deciles, whereas TNn was primarily distributed in the 5th to 8th deciles. The WSDI was predominantly distributed in the 1st decile and then decreased substantially. The total number of ECIs was primarily distributed within the 1st to 5th deciles and gradually decreased toward the 10th decile. Consequently, the distribution of the 35 GCM-SSP combination datasets approximated a right-skewed distribution, suggesting a structured pattern with statistical significance rather than random variability.

Table 4. Decile distribution of extremeness for eight ECIs of all GCM-SSP combinations.

ECI/Decile	Precipitation				Air temperature				Total
	Rx5day	R10mm	CDD	CWD	TXx	TNn	WSDI	DTR	
1st [Min]	489	9	214	725	23	4	1533	22	3019
2nd	1300	176	939	1370	190	21	575	133	4704
3rd	626	657	802	511	654	55	277	499	4081
4th	233	981	471	134	914	134	145	992	4004
5th	97	635	215	39	640	418	103	735	2882
6th	32	263	91	14	251	736	55	271	1713
7th	14	59	42	6	84	755	34	105	1099
8th	6	18	20	0	36	453	34	37	604
9th	2	1	4	0	5	191	25	4	232
10th [Max]	1	1	2	1	3	33	19	2	62

Extremeness scores were calculated using the number of grouped ECIs and their corresponding weights. Group weights were assigned as follows: the first group weighed 1 and the final group weighed 10. For example, if the number of ECI in the 10th group is two, the extremeness score would be 20. Similarly, if the number in the 4th group was 3, the score was 12. In the final step of extreme quantification, only the top 50% of the distribution (6th–10th groups) were used. This top 50% criterion, covering approximately 17% of the 22,400 ECIs, ensured that all the GCM-SSPs were included and designed to reflect the most extreme situations. Figure 7 presents the results of the extremeness quantification for each GCM-SSP combination.

In Figure 7(A), the GFDL has the highest mean extremeness at 1045, although it exhibits a narrow distribution range. Similarly, narrow distributions were observed in the EC3, MPI, and MRI models, suggesting that despite high extremeness levels, information about extremeness across the five SSP scenarios was less diverse. In contrast, Can5 had the second highest mean extremeness at 917, along with the maximum extremeness value, and its extremeness values were widely distributed. This suggests that Can5 combinations provide information about a diverse range of extreme events. For EC3, the mean extremeness was 533, which was the lowest among the models with a narrow distribution range. Consequently, EC3 can be considered to have low extremeness and diversity. Overall, the GCM with high extremeness were Can5, GFDL, and MPI, whereas those with low extremeness were EC3, IPSL, MIR6, and MRI. Compared with the variability of each GCM-SSP combination, the characteristics of each combination were more distinct in terms of extremeness.

The integrated extremeness values for all GCM-SSP combinations were normalized to a range of one to two, as shown in Figure 7(B). The highest value was observed for Can5-SSP585, whereas the lowest was observed for MIR6-SSP585, followed by a significant increase. Notably, no consistent features were observed across SSP scenarios in terms of extreme values. For each GCM, maximum extremeness generally occurred at SSP585 in Can5, GFDL, IPSL, and MPI. Because extremeness values tended to align with more severe scenarios, such as SSP585 or SSP370, these results were expected. However, the highest extreme values for MRI, MI6, and EC3 occurred under SSP119 or SSP126, which represents a strong mitigation of global warming. Interestingly, the second-highest extremeness for the GFDL also occurred at SSP119. Similar to the variability observed in Section 3.2.1, the SSP scenario type did not necessarily produce the expected extreme patterns. These findings were consistent with those of previous studies. Extreme weather and related climate indices are generally higher under SSP585 than under other SSP scenarios (Almazroui et al., 2021; de Vries et al., 2024; Zarrin and Dadashi-Roudbari, 2021; Zhu et al., 2021). However, studies have shown that although SSP585 often exhibits the greatest extremeness, it does not necessarily lead to the highest variability in all cases (Chen and Sun, 2021; Ghazi and Jeihouni, 2022; Wei et al., 2023; Zou and Zhou, 2022). Therefore, it is important to consider all SSP scenarios for each GCM to capture a comprehensive spectrum of possible climate behaviors, including variability and extremeness.

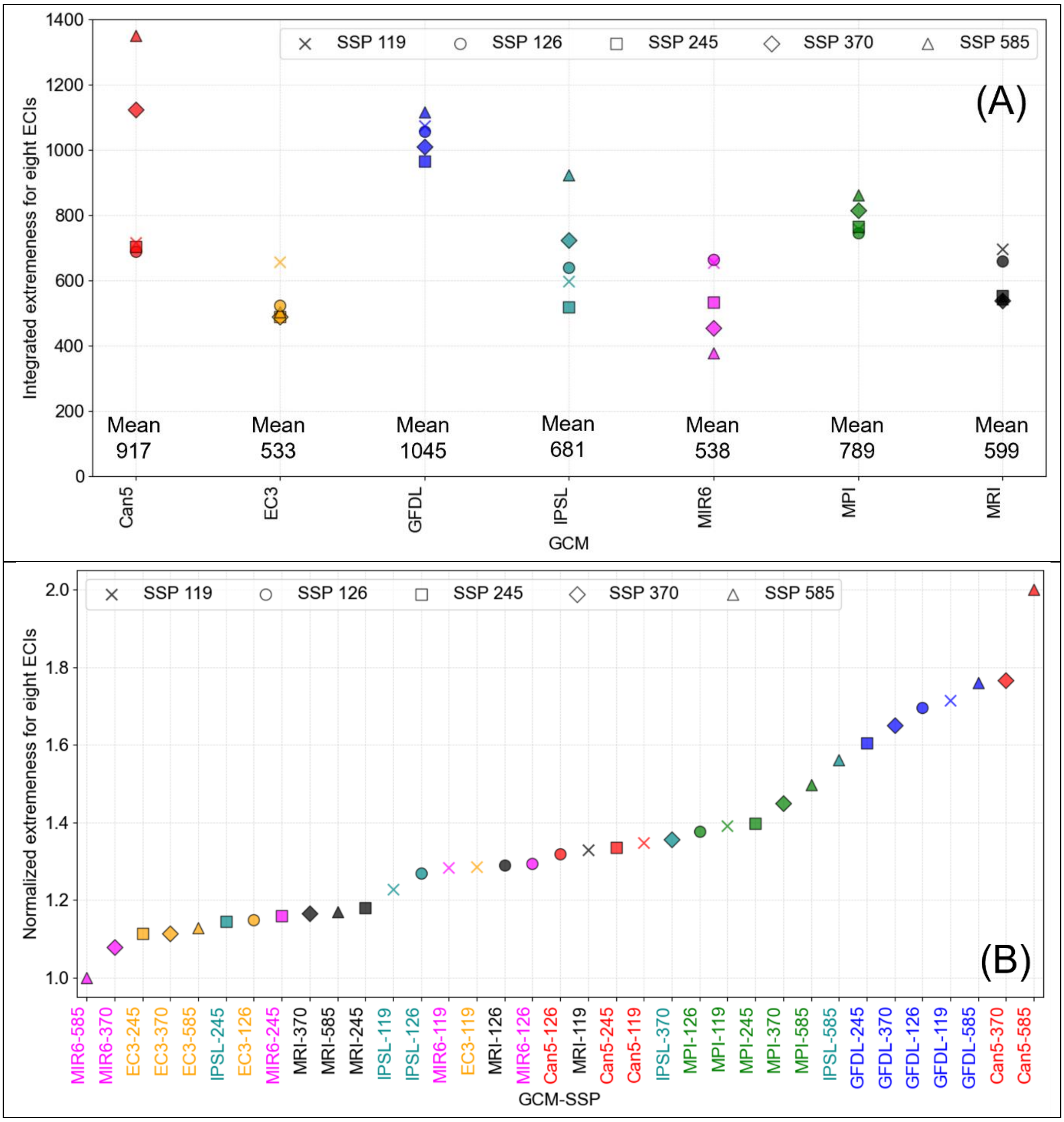

Figure 7. Extremeness score analysis results across all GCM-SSP combinations. (A) Weighted extremeness scores and (B) Normalized weighted extremeness scores.

3.2.3. Integration of variability and extremeness

To quantify the characteristics of each GCM-SSP combination, their variability and extremeness were integrated, as shown in Figure 8. Integrated values ranging from one to four, were calculated by multiplying the normalized variability and extremeness. A higher value indicates both high variability and extremeness in the GCM-SSP combination, suggesting more severe future precipitation and air temperature conditions. The highest integrated values were observed for Can5-SSP585 and GFDL-

SSP585, which were distinct from those of the other combinations because of their significantly higher values. In contrast, a lower value indicates low variability and extremeness, suggesting more mitigated future conditions for precipitation and air temperature. The lowest integrated value was observed for MIR6-SSP370, with no exceptionally low integrated values.

One notable observation in Figure 8 is that, above the median of the integrated values, the values generally increased from SSP119 to SSP585. However, this trend was less pronounced below the median, with some cases showing even higher MIR6 values under SSP119 or SSP126. These results suggest that the SSP scenarios can be clearly distinguished based on their high variability and extremeness, whereas their characteristics may appear less distinct under conditions of low variability and extremeness. Although it was initially expected that both the variability and extremes would increase under the SSP585 scenario, this was not always the case. Similarly, SSP585 did not necessarily produce the highest values for integrated variability and extremeness.

These findings indicate that it may not be appropriate to select climate change scenarios for aquatic environmental impact assessments based solely on a specific GCM or SSP. Each GCM-SSP combination should be treated as a distinct model scenario, as relying on a single GCM or SSP may overlook the inherent uncertainties in climate projections (Pirani et al., 2024; Poole, 2001). Different GCMs and SSPs can yield varied outcomes, even under similar boundary conditions, leading to distinct impacts on the aquatic environment. Therefore, treating each GCM-SSP combination as a unique scenario is critical for capturing the full range of potential futures.

In this study, variability and extremeness were integrated across multiple regions over long periods. This approach can be followed by a thorough analysis of the scenario characteristics for specific local areas after the scenario selection. This is because even if the overall variability and extremeness are high, some parts of the time and spatial domains can have relatively lower values of variability and extremeness. As reported in numerous studies, the variability can vary across regions (Almazroui et al., 2021; Das et al., 2022; Wei et al., 2023; Zarrin and Dadashi-Roudbari, 2021; Zhu et al., 2021; Zou and Zhou, 2022). Additionally, when downscaling from global-scale to local-scale models, issues such as bias, non-stationarity, overfitting, and uncertainty propagation can occur (Chokkavarapu and Mandla, 2019), making it important to evaluate variability and extremeness at the global scale. Similarly, as climate model uncertainties increase over longer timeframes (Kundzewicz et al., 2018), uncertainties in both variability and extremeness may also increase when analyzing long-term trends.

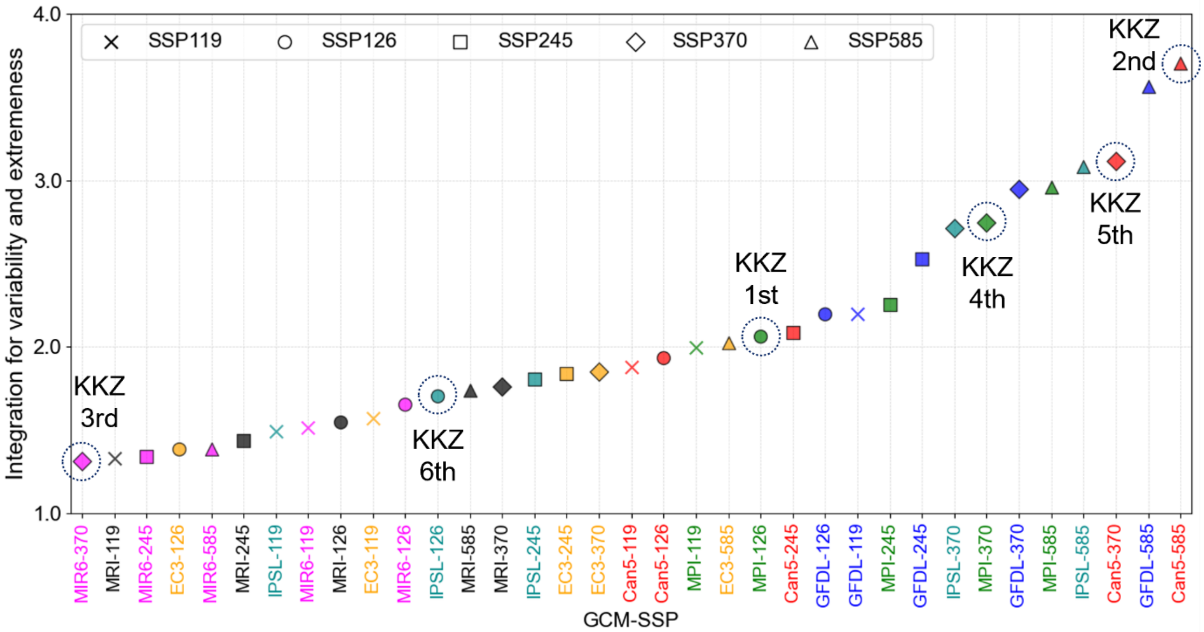

Figure 8. GCM-SSP characterization by integrating variability and extremeness, and selected combinations using the KKZ algorithm.

3.3. Selection of SSP scenarios using the KKZ algorithm

The selection of climate change scenarios for the water environment impact assessments was conducted using the KKZ algorithm. Figure 8 shows the six selected GCM-SSP combinations. MPI-SSP126 was chosen as the first model because it was closest to the centroid of the model ensemble, representing the average behavior of all models (Seo et al., 2019). Can5-SSP585, selected as the second model, and MIR6-SSP370, as the third, represent the maximum and minimum extremes, respectively. These models are the most distinctive in terms of variability and extremeness. Using only these three combinations makes it possible to capture the fullest range of precipitation and air temperature variability and extremes across climate scenarios while also reflecting the average conditions. Nonetheless, the fourth, fifth, and subsequent combinations provided complementary information, bridging the gap between the second and third models.

One important consideration is whether to include or exclude values that appear to be outliers when selecting scenarios. As shown in Figure 8, Can5-SSP585 and GFDL-SSP595 had slightly larger values than the other combinations. If these two combinations are considered outliers and excluded, the model selection results obtained using the KKZ algorithm will change. This is particularly relevant because the KKZ algorithm uses the centroid model as a reference point to determine the next model. Therefore, it is crucial to consider circumstances that may influence the selection of a central model. In most other studies (Cannon, 2015; Farjad et al., 2019; Qian et al., 2021; Ross and Najjar, 2019; Seo et al., 2019), the KKZ algorithm was applied using multidimensional data. However, as the number of dimensions increased, visually identifying outliers became significantly more difficult. In this study, although only two variables—variability and extremeness—were used, the dimensionality was reduced by integrating them into a single value, making outlier detection easier. In the future, even if more characteristics explaining climate change scenarios are introduced, reducing the dimensionality to an integrated value could provide an integrated understanding of the scenarios and identify outliers.

4. Conclusion

This study aimed to develop an approach for identifying suitable GCM-SSP combinations for climate change assessments in aquatic environments. Each GCM-SSP combination was treated as an individual scenario without assigning any special significance to either the GCM or SSP. The key components of this approach are variability and the extremeness of climate-change projections. These two components were integrated into a single value to represent the unique characteristics of each GCM-SSP combination. The KKZ algorithm was then used to determine the optimal selection of GCM-SSP combination. This approach captures the largest range of climate change impacts on aquatic environments by selecting an appropriate number of scenarios, that is, a small part of all GCM-SSP combinations.

Several other studies selected climate change scenarios based on specific GCMs, SSPs, and statistical calculations. These include methods such as change rates, averages, and variances of precipitation and air temperature as well as composite approaches such as clustering, Principal Component Analysis, and the KKZ algorithm combined with ECIs (Cannon, 2015; Carvalho et al., 2016; Farjad et al., 2019; Hong and Ying, 2018; Lee and Kim, 2012; Lutz et al., 2016; Qian et al., 2021; Seo et al., 2019). In addition to these established methods, the approach proposed in this study integrates extensive climate change data across multiple sites, time periods, and indices by characterizing the variability and extremeness of precipitation and air temperature. Additionally, while this study focused on ECIs related to precipitation and air temperature, it is also possible to include other weather indices such as wind, relative humidity, and solar radiation. That is, the approach is expandable and includes both spatial and temporal dimensions. Overall, the suggested approach focuses on diverse situations and extreme events that climate change can trigger. Based on this approach, the impact assessment of aquatic environments using selected climate change scenarios can provide comprehensive information for adaptation strategies from the perspectives of variability and extreme climate change. Furthermore, this methodology can be applied to other environmental domains such as agriculture or infrastructure by adopting relevant climate proxy variables. Thus, future studies could expand this approach by incorporating additional climate variables or focusing on specific climate impacts, thereby enhancing its applicability to broader climate adaptation efforts.

Data availability

Data will be made available on request.

Competing Interest

The authors declare that they have no conflict of interest.

Acknowledgement

This work was supported by Korea Environment Industry & Technology Institute (KEITI) through Climate Change R&D Project for New Climate Regime, funded by Korea Ministry of Environment (MOE) (RS-2022-KE002152).

Reference

1. Almazroui, M., Saeed, F., Saeed, S., Ismail, M., Ehsan, M.A., Islam, M.N., Abid, M.A., O'Brien, E., Kamil, S. and Rashid, I.U. 2021. Projected changes in climate extremes using CMIP6 simulations over SREX regions. Earth Systems and Environment 5(3), 481-497. https://doi.org/10.1007/s41748-021-00250-5.
2. Biemans, H., Speelman, L., Ludwig, F., Moors, E., Wiltshire, A., Kumar, P., Gerten, D. and Kabat, P. 2013. Future water resources for food production in five South Asian river basins and potential for adaptation—A modeling study. Science of the Total Environment 468, S117-S131. https://doi.org/10.1016/j.scitotenv.2013.05.092.
3. Boucher, O., Servonnat, J., Albright, A.L., Aumont, O., Balkanski, Y., Bastrikov, V., Bekki, S., Bonnet, R., Bony, S. and Bopp, L. 2020. Presentation and evaluation of the IPSL-CM6A-LR climate model. Journal of Advances in Modeling Earth Systems 12(7), e2019MS002010. https://doi.org/10.1029/2019MS002010.
4. Cannon, A.J. 2015. Selecting GCM scenarios that span the range of changes in a multimodel ensemble: Application to CMIP5 climate extremes indices. Journal of Climate 28(3), 1260-1267. https://doi.org/10.1175/JCLI-D-14-00636.1.
5. Carvalho, M., Melo-Gonçalves, P., Teixeira, J. and Rocha, A. 2016. Regionalization of Europe based on a K-Means Cluster Analysis of the climate change of temperatures and precipitation. Physics and Chemistry of the Earth, Parts A/B/C 94, 22-28. https://doi.org/10.1016/j.pce.2016.05.001.
6. Chen, H. and Sun, J. 2021. Significant increase of the global population exposure to increased precipitation extremes in the future. Earth's Future 9(9), e2020EF001941. https://doi.org/10.1029/2020EF001941.
7. Chokkavarapu, N. and Mandla, V.R. 2019. Comparative study of GCMs, RCMs, downscaling and hydrological models: a review toward future climate change impact estimation. SN Applied Sciences 1(12), 1698. https://doi.org/10.1007/s42452-019-1764-x.
8. Cooley, A.K. and Chang, H. 2021. Detecting change in precipitation indices using observed (1977–2016) and modeled future climate data in Portland, Oregon, USA. Journal of Water and Climate Change 12(4), 1135-1153. https://doi.org/10.2166/wcc.2020.043.

9. Das, S., Kamruzzaman, M. and Islam, A.R.M.T. 2022. Assessment of characteristic changes of regional estimation of extreme rainfall under climate change: A case study in a tropical monsoon region with the climate projections from CMIP6 model. Journal of hydrology 610, 128002. https://doi.org/10.1016/j.jhydrol.2022.128002.

10. de Vries, I., Sippel, S., Zeder, J., Fischer, E. and Knutti, R. 2024. Increasing extreme precipitation variability plays a key role in future record-shattering event probability. Communications Earth & Environment 5(1), 482. https://doi.org/10.1038/s43247-024-01622-1.

11. Döscher, R., Acosta, M., Alessandri, A., Anthoni, P., Arneth, A., Arsouze, T., Bergmann, T., Bernadello, R., Bousetta, S. and Caron, L.-P. 2021. The EC-earth3 Earth system model for the climate model intercomparison project 6. Geoscientific Model Development Discussions 2021, 1-90. https://doi.org/10.5194/gmd-15-2973-2022.

12. Dunne, J.P., Horowitz, L., Adcroft, A., Ginoux, P., Held, I., John, J., Krasting, J.P., Malyshev, S., Naik, V. and Paulot, F. 2020. The GFDL Earth System Model version 4.1 (GFDL-ESM 4.1): Overall coupled model description and simulation characteristics. Journal of Advances in Modeling Earth Systems 12(11), e2019MS002015. https://doi.org/10.1029/2019MS002015.

13. Eum, H.-I., Kim, J.P. and Cho, J. 2018. High-resolution climate data from an improved GIS-based regression technique for South Korea. KSCE Journal of Civil Engineering 22, 5215-5228. https://doi.org/10.1007/s12205-017-1441-9.

14. Farjad, B., Gupta, A., Sartipizadeh, H. and Cannon, A. 2019. A novel approach for selecting extreme climate change scenarios for climate change impact studies. Science of the Total Environment 678, 476-485. https://doi.org/10.1016/j.scitotenv.2019.04.218.

15. Ghazi, B. and Jeihouni, E. 2022. Projection of temperature and precipitation under climate change in Tabriz, Iran. Arabian Journal of Geosciences 15(7), 621. https://doi.org/10.1007/s12517-022-09848-z.

16. Greenland, S., Senn, S.J., Rothman, K.J., Carlin, J.B., Poole, C., Goodman, S.N. and Altman, D.G. 2016. Statistical tests, P values, confidence intervals, and power: a guide to misinterpretations. European journal of epidemiology 31(4), 337-350. https://doi.org/10.1007/s10654-016-0149-3.

17. Hong, Y. and Ying, S. 2018. Characteristics of extreme temperature and precipitation in China in 2017 based on ETCCDI indices. Advances in Climate Change Research 9(4), 218-226. https://doi.org/10.1016/j.accre.2019.01.001.

18. Katsavounidis, I., Kuo, C.-C.J. and Zhang, Z. 1994. A new initialization technique for generalized Lloyd iteration. IEEE Signal processing letters 1(10), 144-146. https://doi.org/10.1109/97.329844.

19. Kundzewicz, Z.W., Krysanova, V., Benestad, R., Hov, Ø., Piniewski, M. and Otto, I.M. 2018. Uncertainty in climate change impacts on water resources. Environmental Science & Policy 79, 1-8. https://doi.org/10.1016/j.envsci.2017.10.008.

20. Lee, J.-K. and Kim, Y.-O. 2012. Selecting climate change scenarios reflecting uncertainties. Atmosphere 22(2), 149-161. https://doi.org/10.14191/Atmos.2012.22.2.149.

21. Lutz, A.F., ter Maat, H.W., Biemans, H., Shrestha, A.B., Wester, P. and Immerzeel, W.W. 2016. Selecting representative climate models for climate change impact studies: an advanced envelope-based selection approach. https://doi.org/10.1002/joc.4608.

22. Mahlstein, I. and Knutti, R. 2010. Regional climate change patterns identified by cluster analysis. Climate dynamics 35(4), 587-600. https://doi.org/10.1007/s00382-009-0654-0.

23. Mauritsen, T., Bader, J., Becker, T., Behrens, J., Bittner, M., Brokopf, R., Brovkin, V., Claussen, M., Crueger, T. and Esch, M. 2019. Developments in the MPI-M Earth System Model version 1.2 (MPI-ESM1. 2) and its response to increasing CO2. Journal of Advances in Modeling Earth Systems 11(4), 998-1038. https://doi.org/10.1029/2018MS001400.

24. McSweeney, C., Jones, R., Lee, R.W. and Rowell, D. 2015. Selecting CMIP5 GCMs for downscaling over multiple regions. Climate Dynamics 44, 3237-3260. https://doi.org/10.1007/s00382-014-2418-8.

25. Mendlik, T. and Gobiet, A. 2016. Selecting climate simulations for impact studies based on multivariate patterns of climate change. Climatic change 135, 381-393. https://doi.org/10.1007/s10584-015-1582-0.

26. Najafi, M.R. and Moradkhani, H. 2015. Multi-model ensemble analysis of runoff extremes for climate change impact assessments. Journal of Hydrology 525, 352-361. https://doi.org/10.1016/j.jhydrol.2015.03.045.

27. Pirani, A., Fuglestvedt, J.S., Byers, E., O'Neill, B., Riahi, K., Lee, J.-Y., Marotzke, J., Rose,

S.K., Schaeffer, R. and Tebaldi, C. 2024. Scenarios in IPCC assessments: lessons from AR6 and opportunities for AR7. npj Climate Action 3(1), 1. https://doi.org/10.1038/s44168-023-00082-1.

28. Poole, C. 2001. Low P-values or narrow confidence intervals: which are more durable? Epidemiology 12(3), 291-294.

29. Qian, B., Jing, Q., Cannon, A.J., Smith, W., Grant, B., Semenov, M.A., Xu, Y.-P. and Ma, D. 2021. Effectiveness of using representative subsets of global climate models in future crop yield projections. Scientific Reports 11(1), 20565. https://doi.org/10.1038/s41598-021-99378-7.

30. Ross, A.C. and Najjar, R.G. 2019. Evaluation of methods for selecting climate models to simulate future hydrological change. Climatic Change 157(3), 407-428. https://doi.org/10.1007/s10584-019-02512-8.

31. Samadi, S.Z., Sagareswar, G. and Tajiki, M. 2010. Comparison of general circulation models: methodology for selecting the best GCM in Kermanshah Synoptic Station, Iran. International Journal of Global Warming 2(4), 347-365. https://doi.org/10.1504/IJGW.2010.03759.

32. Seo, S.B. and Kim, Y.-O. 2018. Impact of spatial aggregation level of climate indicators on a national-level selection for representative climate change scenarios. Sustainability 10(7), 2409. https://doi.org/10.3390/su10072409.

33. Seo, S.B., Kim, Y.-O., Kim, Y. and Eum, H.-I. 2019. Selecting climate change scenarios for regional hydrologic impact studies based on climate extremes indices. Climate Dynamics 52, 1595-1611. https://doi.org/10.1007/s00382-018-4210-7.

34. Shannon, C.E. 1948. A mathematical theory of communication. The Bell system technical journal 27(3), 379-423. https://doi.org/10.1002/j.1538-7305.1948.tb01338.x.

35. Stocker, T.F., Qin, D., Plattner, G.-K., Alexander, L.V., Allen, S.K., Bindoff, N.L., Bréon, F.-M., Church, J.A., Cubasch, U. and Emori, S. (2013) Climate change 2013: the physical science basis. Contribution of Working Group I to the Fifth Assessment Report of the Intergovernmental Panel on Climate Change, pp. 33-115, Cambridge University Press.

36. Swart, N.C., Cole, J.N., Kharin, V.V., Lazare, M., Scinocca, J.F., Gillett, N.P., Anstey, J., Arora,

V., Christian, J.R. and Hanna, S. 2019. The Canadian earth system model version 5 (CanESM5. 0.3). Geoscientific Model Development 12(11), 4823-4873. https://doi.org/10.5194/gmd-12-4823-2019.

37. Tatebe, H., Ogura, T., Nitta, T., Komuro, Y., Ogochi, K., Takemura, T., Sudo, K., Sekiguchi, M., Abe, M. and Saito, F. 2019. Description and basic evaluation of simulated mean state, internal variability, and climate sensitivity in MIROC6. Geoscientific Model Development 12(7), 2727-2765. https://doi.org/10.5194/gmd-12-2727-2019.

38. Thiessen, A.H. 1911. Precipitation averages for large areas. Monthly weather review 39(7), 1082-1089. https://doi.org/10.1175/1520-0493(1911)39<1082b:PAFLA>2.0.CO;2.

39. Vano, J.A., Kim, J.B., Rupp, D.E. and Mote, P.W. 2015. Selecting climate change scenarios using impact-relevant sensitivities. Geophysical Research Letters 42(13), 5516-5525. https://doi.org/10.1002/2015GL063208.

40. Wei, L., Xin, X., Li, Q., Wu, Y., Tang, H., Li, Y. and Yang, B. 2023. Simulation and projection of climate extremes in China by multiple Coupled Model Intercomparison Project Phase 6 models. International Journal of Climatology 43(1), 219-239. https://doi.org/10.1002/joc.7751.

41. Yukimoto, S., Kawai, H., Koshiro, T., Oshima, N., Yoshida, K., Urakawa, S., Tsujino, H., Deushi, M., Tanaka, T. and Hosaka, M. 2019. The Meteorological Research Institute Earth System Model version 2.0, MRI-ESM2. 0: Description and basic evaluation of the physical component. Journal of the Meteorological Society of Japan. Ser. II 97(5), 931-965. https://doi.org/10.2151/jmsj.2019-051.

42. Zarrin, A. and Dadashi-Roudbari, A. 2021. Projection of future extreme precipitation in Iran based on CMIP6 multi-model ensemble. Theoretical and Applied Climatology 144, 643-660. https://doi.org/10.1007/s00704-021-03568-2.

43. Zhang, X., Alexander, L., Hegerl, G.C., Jones, P., Tank, A.K., Peterson, T.C., Trewin, B. and Zwiers, F.W. 2011. Indices for monitoring changes in extremes based on daily temperature and precipitation data. Wiley Interdisciplinary Reviews: Climate Change 2(6), 851-870. https://doi.org/10.1002/wcc.147.

44. Zhu, X., Lee, S.-Y., Wen, X., Ji, Z., Lin, L., Wei, Z., Zheng, Z., Xu, D. and Dong, W. 2021. Extreme climate changes over three major river basins in China as seen in CMIP5 and CMIP6. Climate Dynamics 57, 1187-1205. https://doi.org/10.1007/s00382-021-05767-z.

45. Zou, L. and Zhou, T. 2022. Mean and extreme precipitation changes over China under SSP scenarios: results from high-resolution dynamical downscaling for CORDEX East Asia. Climate Dynamics 58(3), 1015-1031. https://doi.org/10.1007/s00382-021-05947-x.